

Comment on Li et al., *Phys. Medica* 69 (2020) 147-163 “Intercomparison of dose enhancement ratio and secondary electron spectra for gold nanoparticles irradiated by X-rays calculated using multiple Monte Carlo simulation codes” regarding the magnitude of dose enhancement ratios

H. Rabus^{1,12}, W.B. Li^{2,12}, C. Villagrasa^{3,12}, J. Schuemann⁴, P.A. Hepperle^{5,6}, L. de la Fuente Rosales^{5,12}, M. Beuve⁷, S. Di Maria^{8,12}, A.P. Klapproth^{2,9}, F. Poignant^{7,10}, B. Rudek^{4,5,11}, H. Nettelbeck^{5,12}

¹ *Physikalisch-Technische Bundesanstalt, Berlin, Germany*

² *Institute of Radiation Medicine, Helmholtz Zentrum München - German Research Center for Environmental Health, Neuherberg, Germany*

³ *Institut de Radioprotection et de Sûreté Nucléaire, Fontenay-Aux-Roses, France*

⁴ *Massachusetts General Hospital & Harvard Medical School, Department of Radiation Oncology, Boston, MA, USA*

⁵ *Physikalisch-Technische Bundesanstalt, Braunschweig, Germany*

⁶ *Leibniz Universität Hannover, Hannover, Germany*

⁷ *Institut de Physique Nucléaire de Lyon, Université Claude Bernard Lyon 1, Villeurbanne, France*

⁸ *Centro de Ciências e Tecnologias Nucleares, Instituto Superior Técnico, Universidade de Lisboa, Bobadela LRS, Portugal*

⁹ *TranslaTUM, Klinikum rechts der Isar, Technische Universität München, Munich, Germany*

¹⁰ *NASA Langley Research Center, Hampton, VA, USA*

¹¹ *Perlmutter Cancer Center, NYU Langone Health, New York City, NY, USA*

¹² *European Radiation Dosimetry Group (EURADOS) e.V., Neuherberg, Germany*

Abstract

In our paper in *Phys. Medica* 69 (2020) 147-163, we reported results of a Monte Carlo code intercomparison exercise for simulations of the dose enhancement from a gold nanoparticle (GNP) irradiated by X-rays. To highlight potential differences between codes, the dose enhancement ratios (DERs) were shown for the narrow-beam geometry used in the simulations, which leads to values significantly higher than unity over distances in the order of several tens of micrometers from the GNP surface. As it has come to our attention that the figures in our paper have given rise to misinterpretation as showing ‘the’ DERs of GNPs under diagnostic X-ray irradiation, this comment presents estimates of the DERs that would have been obtained with realistic radiation field extensions and presence of secondary particle equilibrium (SPE). These DER values are much smaller than those for a narrow-beam irradiation shown in our paper, and significant dose enhancement is only found within a few hundred nanometers around the GNP.

1. Introduction

In our recent paper 1, we reported on preliminary results of an exercise organized as a joint activity of Working Groups 7 “Internal Dosimetry” and 6 “Computational Dosimetry” of the European Radiation Dosimetry Group 2, 3. The exercise was an intercomparison of Monte Carlo simulations for the case of dose enhancement from gold nanoparticles (GNP) under X-ray irradiation.

GNPs are considered as potential radiosensitizers in the field of radiation therapy 4, 5, 6, 7, 8, 9, as they have been shown to enhance the biological radiation effectiveness in vitro and in vivo 4, 9, 10, 11. This effect is often explained by a local enhancement of absorbed dose around GNPs that results from the higher absorption of radiation by the high-Z material gold as compared to biological matter or water. Due to the stronger interaction with the incoming photons and ensuing Auger cascades, a larger number of secondary electrons will be emitted from the GNP and deposit additional energy in its vicinity as compared to the case when the GNP volume is also filled with water. The ratio of the absorbed dose within water volumes

surrounding the GNP for the two cases of GNP present or absent is the dose enhancement ratio (DER).

The dose enhancement from GNPs is limited to microscopic dimensions and, therefore, requires determination by theoretical methods or by Monte Carlo (MC) simulations. The small size of GNPs of typically a few tens of nanometers imposes a major challenge on such MC simulations. The exercise reported in 1 aimed at studying the dependence of the results on both the MC codes used and the choice of adjustable parameters (cut-off energies, cross section models, etc.; see Table 1 in 1). For this purpose, a photon beam with a cross sectional area comparable to that of the GNP was used in the simulations. In this way, differences between codes such as in the interaction cross sections and implementation of electron transport in gold are emphasized. Furthermore, the range of photon energies was chosen such as to have maximum differences between photon interaction cross sections for gold and water.

Participants in the exercise were requested to simulate the irradiation of a single spherical gold nanoparticle surrounded by water with a parallel photon beam of circular cross section. The photon source was placed at a distance of 100 μm from the GNP

and had a diameter of 60 nm or 110 nm for a GNP diameter of 50 nm or 100 nm, respectively. Two X-ray spectra were considered that corresponded to tube voltages of 50 kVp and 100 kVp (for details see 1).

For all combinations of photon energy spectrum and GNP size, simulations were performed (a) with the GNP in place and surrounded by water and (b) with the respective volume only filled with liquid water. Energy deposition was scored in spherical water shells around the GNP volume. Up to 1 μm from the GNP surface, the spherical shells had a thickness of 10 nm, and between 1 μm and 50 μm the shell thickness was 1 μm . DERs were determined as the ratio of the energies deposited in each spherical shell in the simulations with GNP and for water only. In addition, participants were also requested to report the energy spectra of electrons emitted from the GNP for all combinations of GNP size and photon spectrum.

The DERs presented in 1 were significantly higher than unity over distances in the order tens of micrometers from the GNP surface. For instance, in Fig. 6(d) in 1 all reported DERs for the 100 nm GNP and 100 kVp X-ray spectrum are higher than 1.5 up to 20 μm distance. If the same dose enhancement would also be found in broad beam irradiation, this would mean that the presence of a single 100 nm GNP during irradiation would lead to a 50% increase of absorbed dose in a cell. This is unrealistic as (assuming a cell diameter of 10 μm) the mass fraction of gold would be about 2×10^{-5} , and thus, with up to 100 times higher mass energy absorption of gold compared to water 12, the dose enhancement cannot exceed the order of 0.2%.

It is well known that results for DERs are highly dependent on the simulation setup 13, 14, 15 and it was clearly stated in 1 that the shown DERs are valid only for the particular exposure scenario that was used for the simulations. As it has come to our attention that the results reported in 1 are prone to be misinterpreted at representing ‘the’ DERs of GNPs under diagnostic X-ray irradiation, this comment is to counteract this misinterpretation by showing how much different the DERs would be for a GNP irradiated with an extended photon field.

2. Materials and Methods

2.1. Physical background

If simulations are carried out using a photon beam of microscopic cross section, then the energy imparted in the scoring volumes is predominantly deposited by electron tracks produced within the region traversed by the primary photon beam. In the exercise of 1, this region was a water cylinder of about 100 μm height (diameter of the scoring region) with or without the presence of a GNP within. The mass fraction of gold was in the order of 1% to 2% and this high mass fraction of gold was the reason for the large DERs and extended spatial range, where DERs were significantly larger than unity.

In an extended photon field, electrons generated by photon interactions outside the volume, which is defined by the beam direction and GNP cross section, also deposit energy in the vicinity of the GNP. In case of secondary charged particle equilibrium (CPE), that is if the energy transported out of a volume by leaving electrons equals the energy introduced in the volume by entering electrons, the absorbed dose is equal to the energy released in photon interactions in that volume.

Over microscopic dimensions where the attenuation of the photon beam can be neglected, the absorbed dose then has a constant value. In the presence of the GNP, the conditions of CPE are not met for the volume of the GNP, as the gold atoms are greater absorbers than water molecules, and thus, more energy is transported by electrons out of the GNP volume than into it.

For an extended photon beam, photons scattered outside the confined volume (defined by beam direction and GNP cross section) can also reach the GNP and have interactions with it or within its vicinity. The electrons released by interactions of these scattered photons in the GNP or its surroundings increase the energy deposited in the regions of interest.

Hence, in simulations with confined beams, the lack of CPE together with the absence of interactions of scattered photons in the water volume around the GNP leads to an increase in the DER, while neglecting the interactions of scattered photons with the GNP leads to a slight reduction in the DER.

A procedure to use the results of such simulations to derive the DER for an extended photon field was described in detail in 16. It is based on two assumptions that are briefly reviewed in the next two subsections: one is related to the correction for the lack of charge particle equilibrium (CPE) and one to the lack of secondary photon equilibrium (SPE).

2.2. Correction for lack of charged particle equilibrium (CPE)

The first assumption is that the lack of energy deposition in the water shells around the GNP from electrons originating from outside the confined beam geometry is the same with and without the GNP present. This assumption means that the difference of energy per mass obtained from the simulations with and without the GNP can be used as value for the extra contribution coming from the GNP. This contribution then adds to the dose to water, D_w , in the absence of the GNP, which on the conditions of CPE is equal to the collision kerma 17

$$D_w = \int E \times \frac{\mu_{en,w}(E)}{\rho} \times \Phi(E) e^{-\mu_w(E)d_g} dE \quad (1)$$

where E is the photon energy, $\mu_{en,w}(E)/\rho$ is the mass energy absorption coefficient of water, $\Phi(E)$ is the spectral fluence (particles per area and energy interval) of photons in the region of interest (i.e. around the GNP position), $\mu_w(E)$ is the total linear attenuation coefficient of water and d_g is the distance of the GNP volume center from the photon source. As the attenuation of the photon beam is negligible over the microscopic dimensions considered, the absorbed dose to water is constant in the absence of the GNP.

In the presence of the GNP, there is additional energy deposition from electrons emerging from the GNP, while the energy deposition from electrons produced in the same volume in water when the GNP is absent is missing. The simulation results of deposited energy in the spherical shells around the GNP are basically the sum of aforementioned contributions and the energy depositions from electrons released by photon interaction in the rest of the volume traversed by the beam (except the sphere covered by the GNP or filled with water). Therefore, the difference of the simulation results for the cases with and without the GNP can be used as approximation for the extra dose contribution due to the GNP.

With this approximation, the CPE-corrected dose $D_g^{(p)}(r)$ in a spherical shell between radial distances r and $r+\Delta r$ from the GNP surface is approximately given by

$$D_g^{(p)}(r) = D_w^{(p)} + \frac{\bar{\varepsilon}_g(r) - \bar{\varepsilon}_w(r)}{m_w(r)} \quad (2)$$

In eq. (2), $D_w^{(p)}$ is the dose to water under CPE conditions calculated with eq. (1) using the primary photon spectral fluence $\Phi^{(p)}$ with the normalization condition

$$\int \Phi^{(p)}(E)dE = \frac{1}{r_b^2 \pi} \quad (3)$$

where r_b is the radius of the circular photon source used in the simulations. $\bar{\varepsilon}_g(r)$ and $\bar{\varepsilon}_w(r)$ in eq. (2) are the average imparted energies per primary photon obtained in the simulations with the GNP and without the GNP, respectively, and $m_w(r)$ is the mass of water in the spherical shell, which is given by

$$m_w(r) = \rho_w 4\pi(r_g + r)^2 \Delta r \quad (4)$$

where ρ_w is the mass density of water and r_g is the GNP radius.

2.3. Correction for lack of scattered photon equilibrium (SPE)

The second assumption is that the excess dose $D_g^{(s)}$ due to photons produced (in an extended photon beam) by scattering interactions outside the confined beam geometry that interact with the GNP can be estimated by multiplying the difference between simulations with and without the GNP using a scaling factor. This scaling factor is the ratio of the collision kermas in gold for the energy spectra of scattered photons and for the primary photon spectrum, $D_{Au}^{(s)}$ and $D_{Au}^{(p)}$, respectively, i.e.

$$D_g^{(s)}(r) = D_w^{(s)} + \frac{\bar{\varepsilon}_g(r) - \bar{\varepsilon}_w(r)}{m_w(r)} \frac{D_{Au}^{(s)}}{D_{Au}^{(p)}} \quad (5)$$

where $D_w^{(s)}$ is the dose to water calculated with eq. (1) using the spectral fluence of scattered photons, $\Phi^{(s)}$, and the collision kerma in gold is calculated according to

$$D_{Au} = \int E \times \frac{\mu_{en,Au}(E)}{\rho} \times \Phi(E)dE \quad (6)$$

where $\mu_{en,Au}(E)/\rho$ is the mass energy absorption coefficient of gold. The approximation is that the dose deposited in water around the GNP scales with the collision kerma of photon interactions inside the GNP. As the electrons released by photon interactions in the GNP lose part of their energy in the GNP, there may be a dependence on the size of the GNP and the photon energy spectrum.

The spectral fluence of scattered photons that reach the GNP can be determined analytically only for the case that exactly one coherent or incoherent scattering event has occurred. The fluence of all generations of scattered photons that reach the GNP is estimated from the ratio of the sum of spectral fluences of all generations of scattered photons to the spectral fluence of the first generation that would be obtained if photon scattering was isotropic. This ratio is multiplied by the spectral fluence of singly scattered photons with the correct angular dependence to

approximate the fluence of all generations of photons scattered with the proper angular dependence 16.

The spectral fluence of singly scattered photons can be calculated by multiplying the following probabilities and integrating over the volume traversed by the extended primary photon beam:

(1) Probability that a primary photon reaches the interaction point without any preceding interactions and that the scattered photon reaches the GNP without further interaction. Both probabilities are given by the Lambert-Beer law using the total photon mass attenuation coefficient that is available from literature 18.

(2) Probability that a coherent or incoherent scattering event occurs per unit length, which is given by the respective mass attenuation coefficients 18.

(3) Probability that the scattering occurs within the solid angle covered by the GNP. This can be estimated from the differential Thomson and Klein-Nishina cross sections 16.

The photon energy spectrum obtained by calculating the fluence of the first generation of scattered photons and scaling to all generations of scattered photons is then used in eq. (1) to calculate the collision kerma due to photon interactions in the volume of the GNP filled with either water or gold by using the respective mass-energy absorption coefficients. Under CPE conditions, the collision kerma obtained for the volume filled with water is equal to the additional dose to water due to the ‘additional’ irradiation with the scattered photons.

The collision kerma obtained for the volume filled with gold is the energy per mass transferred to electrons by photon interactions in gold. The ratio of this collision kerma value (due to the spectrum of scattered photons) and the collision kerma for gold calculated with the primary photon energy spectrum is the factor used to multiply the contribution of the absorbed dose around the GNP (due to photon interactions within the GNP as obtained from the simulations) to estimate the excess dose contribution from electrons released in the GNP by scattered photons 16.

2.4. Consistency checks for the simulation results

For the narrow-beam geometry used in the exercise, the ratio of simulation results with and without GNP present is almost insensitive to normalization as long as it is done consistently in the two simulations for each combination of GNP size and spectrum. On the contrary, the application of the correction for CPE and SPE requires that the simulated data are related to a known primary photon fluence. To ensure that this is the case, the ensemble of reported data (i. e. energy spectra of electrons emitted from the GNP and energy deposition in the spherical shells around it for all combinations of GNP size and photon spectrum) of each participant was subjected to plausibility and consistency checks.

For those sets of results where the consistency tests indicated specific normalization issues, the respective participants were requested to check and confirm whether their simulations were compromised by the respective problem. Examples include improper implementation of the simulation geometry, such as using a source where the radius was larger than the GNP radius by 10 nm rather than applying this difference for the diameters. If the participant confirmed that the simulations were biased as suggested by the outcomes of the consistency checks, the results were corrected accordingly.

A detailed account of this analysis is beyond the scope of this paper and will be published as a comprehensive EURADOS report on the lessons learned from the exercise [19]. For the energy spectra of electrons emitted from the GNP, where the identified normalization issues directly affect the data shown in Figs. 7 and 8 of our original paper 1, a respective corrigendum has been submitted 20.

For the determination of the best estimate for the DER in an extended photon field as well as for the associated uncertainty, we considered in this work only those datasets that passed (from the start or after revision) all three tests described in the next three sub-sections. The best estimate was taken as the mean of these data sets and the associated uncertainty at 95% confidence level was taken as the geometrical mean of twice the sample standard deviation among the accepted results and an estimate for the uncertainty of the corrections (see Section 3.2).

2.5. Criterium for consistency of overall normalization

The first plausibility check was based on the ratio between the total energy $E_{d,w}(R)$ deposited in a sphere of radius R in the simulations without GNP and the average energy $E_{t,w}(R)$ transferred by photon interactions in water occurring in the part of the sphere traversed by the primary photon beam. The latter is given by

$$E_{t,w}(R) = D_w^{(p)} \rho_w r_b^2 \pi \times 2(r_g + R) \quad (7)$$

where the volume traversed by the beam is approximated by a cylinder volume, and $D_w^{(p)}$ is the dose to water calculated with eq. (1) using a primary photon spectral fluence $\Phi^{(p)}$ that satisfies eq. (3).

The deposited energy $E_{d,w}(R)$ for $R=r_j$, where r_j is the outer radius of the j -th spherical shell in the simulations, is approximately given by

$$E_{d,w}(R) = \sum_{i=1}^j \bar{\epsilon}_w(r_i) \quad (8)$$

Here the approximation lies in the fact that the volume corresponding to the GNP is omitted as it has not been used for scoring in the simulations. This approximation is justified, because for values of R in the order of several tens of micrometers, the contribution of the GNP volume filled with water becomes negligible.

With increasing R , the condition of longitudinal secondary electron equilibrium (i.e. along the direction of the primary photon beam) will be fulfilled, such that the ratio $E_{d,w}(R)/E_{t,w}(R)$ should converge with increasing R to a value close to unity. The asymptotic value will not be exactly unity, because the simulation results also include energy deposited by electrons produced in interactions of photons that have been scattered out of the photon beam and of their descendant photons. This effect makes the value of $E_{d,w}(R)$ larger than $E_{t,w}(R)$. Conversely, that the volume of the GNP is not scored leads to a slight reduction, but as this volume is less than 10^{-9} of the total volume and less than 10^{-3} of the volume traversed by the primary beam, this is negligible. Similarly, the fact that a sphere is used for scoring rather than a plane parallel slab will also lead to a slight reduction of $E_{d,w}$ that can be expected to be dependent on the value of R . In fact, the deviation of the ratio $E_{d,w}(R)/E_{t,w}(R)$ from the saturation value approximately showed a $1/R$ dependence for

$R \geq 30 \mu\text{m}$ such that the saturation value could be obtained by linear regression of the ratio as a function of $1/R$.

2.6. Criterium for consistency between emitted electron energy spectra and radial integral of deposited energy

The second plausibility check was whether the difference of the reported energy deposition with GNP present and absent in the spherical shells around the GNP volume was compatible with the energy spectra of electrons emitted from the GNP and with the average energy released in a photon interaction in gold. To test this, (a) the total additional energy $\Delta E_{d,g}$ deposited in the presence of the GNP in the total scoring volume (i. e. a spherical shell of inner radius r_g and outer radius $r_g+50\mu\text{m}$) per photon interaction and (b) the total energy \bar{T} transported out of the GNP by electrons was considered. These two quantities were calculated from eqs. (9) and (10).

$$\Delta E_{d,g}(R = r_j) = \sum_{i=1}^j [\bar{\epsilon}_g(r_i) - \bar{\epsilon}_w(r_i)] \quad (9)$$

$$\bar{T} = \int_0^{T_{max}} T \times \Phi^{(e)}(T) dT \quad (10)$$

In eq. (10), T is the kinetic energy of the electrons and $\Phi^{(e)}$ is their net spectral flux (particles per energy interval), i.e. the difference between electrons leaving and entering the GNP. From energy conservation, if all deposited energy is scored (i. e. for infinitely large R), then $\Delta E_{d,g}$ should be almost identical to \bar{T} , but slightly smaller due to the possibility of emitted electrons being backscattered into the GNP and depositing part of their energy there.

2.7. Criteria for consistency between the data for different GNP size and photon energy spectrum

The third plausibility check was testing whether (a) the total energy $\Delta E_{d,g}^*$ deposited around a GNP in which a photon interaction occurred and/or (b) the total energy \bar{T}^* transported out of such a GNP by electrons were compatible with the average energy E_{tr} transferred to electrons when a photon interacts with a gold atom. E_{tr} depends on the photon energy spectrum and was calculated according to eq. (11).

$$E_{tr} = \frac{\int E \mu_{en,Au}(E) \Phi^{(p)}(E) e^{-\mu_w(E)d_g} dE}{\int \mu_{Au}(E) \Phi^{(p)}(E) e^{-\mu_w(E)d_g} dE} \quad (11)$$

In eq. (11), E is the photon energy, $\mu_{en,Au}$ is the energy absorption coefficient of gold 12, $\Phi^{(p)}$ is the particle fluence of primary photons emitted from the X-ray source, μ_w and μ_{Au} are the photon attenuation coefficients of water and gold 18, and d_g is the distance of the GNP from the photon source. (Strictly speaking, eq. (11) gives a lower bound to the energy transferred to electrons, as they will lose some of their energy by bremsstrahlung collisions.)

$\Delta E_{d,g}^*$ and \bar{T}^* were obtained by dividing $\Delta E_{d,g}(r_{max})$ and \bar{T} by the expected number \bar{n}_g of photon interactions in the GNP, that was calculated from eq. (12)

$$\bar{n}_g = \frac{4\pi}{3} r_g^3 \int \mu_{Au}(E) \times \Phi^{(p)}(E) e^{-\mu_w(E)d_g} dE \quad (12)$$

Table 1 Mean number of photon interactions in a GNP for the two GNP diameters and X-ray radiation qualities used in the exercise. The values apply to the fluences used for normalization of the results in 1. (1 photon per area of the photon source, i.e. per $2.8 \times 10^3 \text{ nm}^2$ and $9.5 \times 10^3 \text{ nm}^2$ for the 50 nm and 100 nm GNPs, respectively.)

	50 kVp	100 kVp
50 nm GNP	1.1×10^{-3}	5.4×10^{-4}
100 nm GNP	2.6×10^{-3}	1.3×10^{-3}

and depends on the GNP size and photon energy spectrum. For a fluence satisfying eq. (3), the values are shown in Table 1. As the electrons released in photon interactions with gold atoms lose part of their energy within the GNP before leaving it, the ratios $\Delta E_{d,g}^*/E_{tr}$ and \bar{T}^*/E_{tr} must be smaller than unity. Furthermore, for the same photon spectrum the ratio should be smaller for the 100 nm GNP than for the 50 nm GNP, as the average path travelled by electrons before leaving the GNP is smaller for the smaller GNP. In addition, for the same GNP size the value for the 100 kVp spectrum should be smaller than for the 50 kVp spectrum, because the electrons produced by photo-absorption in the L, M and outer shells and the Compton

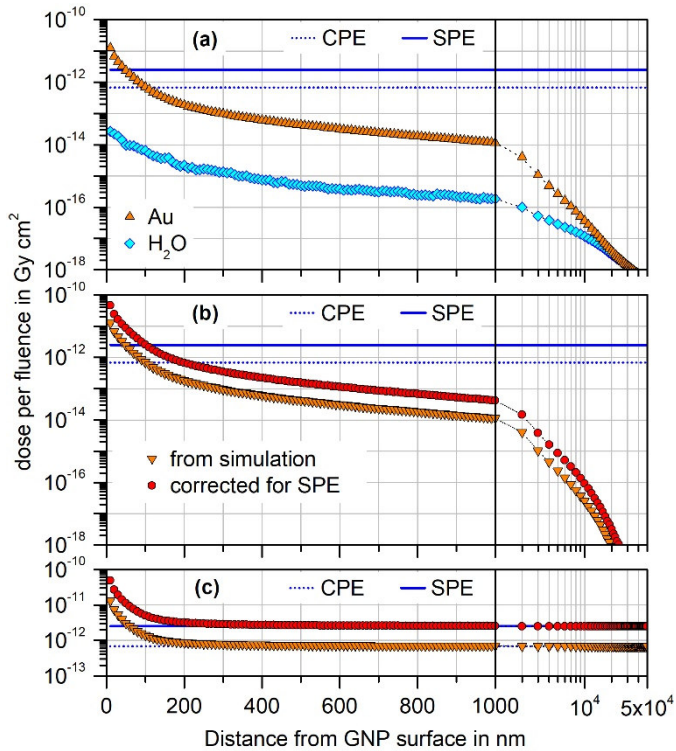


Fig. 1: (a) Simulation results for dose per fluence in spherical shells at different radial distances from a 100 nm gold nanoparticle (GNP) irradiated in water with a circular 50 kVp photon beam of diameter 110 nm (symbols). The x-axis shows the difference between the radius of the spherical shell's outer surface and the GNP radius and is linear up to 1000 nm and then logarithmic. The dashed blue lines on all panels indicate the value obtained without GNP for charged particle equilibrium (CPE); the solid blue lines mark the dose per fluence of primary particles for the case of full secondary particle equilibrium (SPE), i.e. including scattered photons. (b) Difference of the simulation results in (a) for the GNP present and absent (downward triangles) and corrected values taking into account scattered photons (circles). (c) Sums of the data shown in (b) and the constant values of dose to water per fluence for CPE and SPE.

scattered electrons have higher energies. The 100 kVp photon spectrum also contains photon energies where K shell absorption is possible, but the fraction of such photons is small and the photo-absorption coefficient around the K shell of gold is lower than in the photon energy range below 50 keV where the majority of photons in the spectrum are found 18.

3. Results and Discussion

3.1. Application of the corrections to simulated data

The resulting corrections are illustrated in Fig. 1 for the case of a 100 nm GNP irradiated with the 50 kVp X-ray beam, i.e. the combination for which the largest DER values were obtained by all participants in the exercise 1. In Fig. 1, we use the data of a participant whose results were generally around the median of the reported DERs in 1 for each combination of X-ray spectrum and GNP size.

In all three panels of Fig. 1, the dashed line indicates the absorbed dose to water in the absence of the GNP if CPE exists and if only the primary photon spectrum is considered. The solid line is the absorbed dose to water calculated with the estimated fluence of all generations of scattered photons, i.e. under SPE conditions. The results obtained from the simulations with and without the GNP are shown in Fig. 1(a) as symbols (see legend). The difference between these results is shown in Fig. 1(b) as downward triangles, which is approximately equal to the dose contribution in the surrounding water arising from electrons emitted by the GNP following photon interactions. The correction obtained after adding the estimated contribution from scattered photons is indicated by the circles.

Finally, Fig. 1(c) shows the results obtained by adding the estimated dose contributions due to the GNP and the respective estimated dose to water values in the absence of the GNP, when only the correction for CPE is applied (downward triangles) and after accounting also for the correction for SPE (circles).

The DER calculated from the simulation results presented in Fig. 1(a) for the confined beam is shown in Fig. 2 as upward triangles. The squares indicate the DERs obtained after applying the correction for CPE according to eq. (2), and the circles (which are mostly overlapping the squares) are the results from applying the additional correction for scattered photons. From

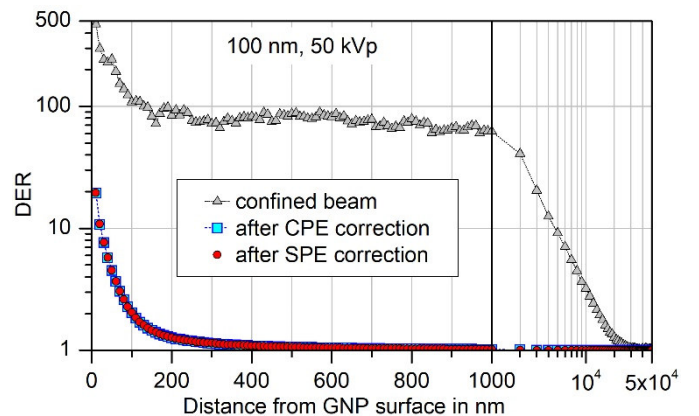


Fig. 2: Dose enhancement ratio (DER) for a 100 nm GNP and 50 kVp X-rays calculated from the data shown in Fig. 1(a) and Fig. 1(c), respectively. The symbols for the results after correcting for CPE (boxes) and after also correcting for SPE (circles) are overlapping.

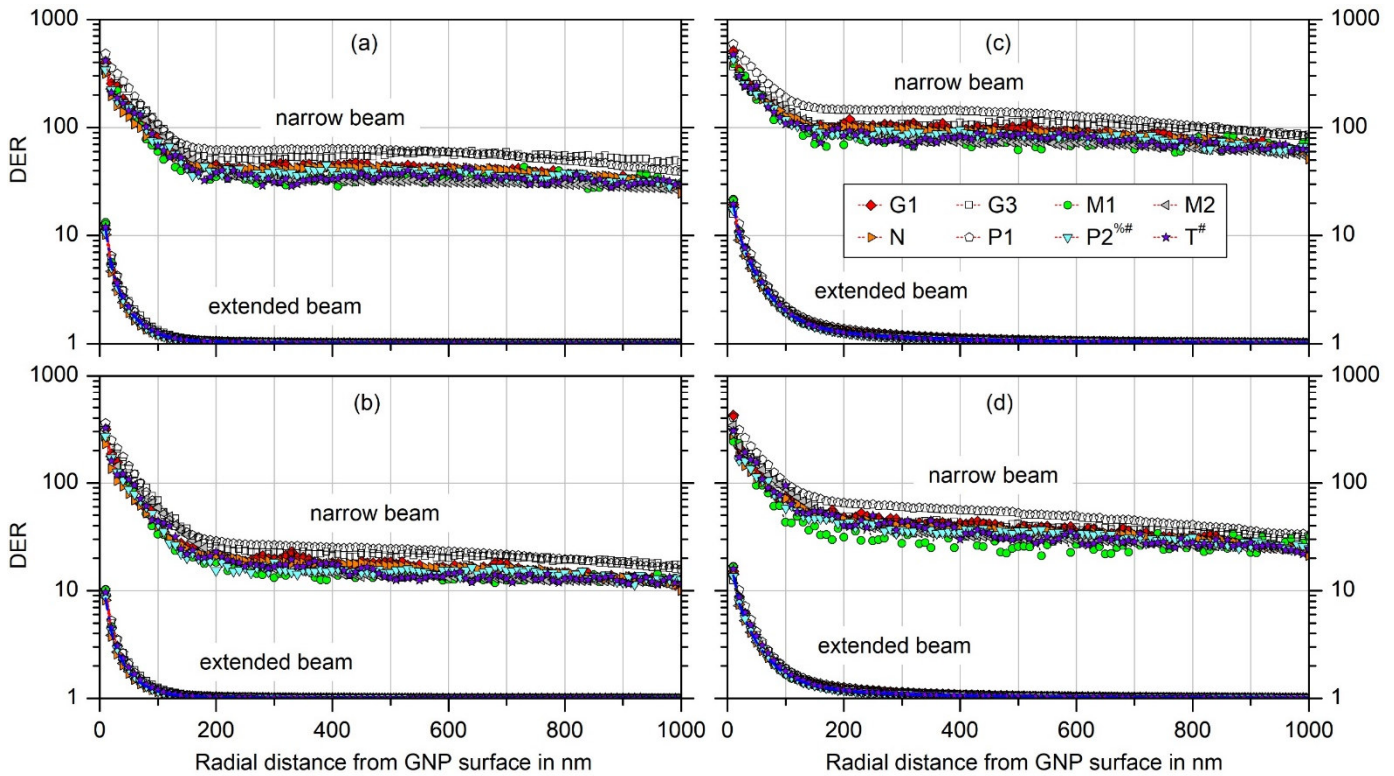


Fig. 3: Comparison of the dose enhancement ratios (DER) for the narrow beam used in the simulations in 1 and for an extended photon field under secondary particle equilibrium for (a) a 50 nm GNP and 50 kVp X-rays, (b) a 50 nm GNP and 100 kVp X-rays, (c) a 100 nm GNP and 50 kVp X-rays and (d) a 100 nm GNP and 100 kVp X-rays. The different symbols correspond to the different participants in the exercise. Open symbols indicate that the reported simulation results did not pass the plausibility checks and no explanation could be reported by the participant. The other data sets passed the plausibility tests, where in some cases identified normalization issues have been corrected for. A hashtag on the participant identifier indicates that a fluence correction was applied on the data (as the photon source geometry was at variance with the exercise definition). A percent sign indicates that results from revised simulations are shown. In both cases, the respective results for the narrow beam differ from those shown in Fig. 4 of 1.

this graph, it is evident that in an extended photon field significant dose enhancement is only found within the first few hundred nanometers around the GNP, and that scattered photons interacting with the GNP do not significantly change the resulting DER.

Fig. 3 shows a comparison between the DERs for a narrow beam and for an extended beam geometry in the range up to 1000 nm from the GNP surface for all combinations of GNP size and X-ray spectrum. The lin-log plots allow a direct comparison with Fig. 4 in 1: In contrast to the significant dose enhancement over micrometers for the confined beam, the DER drops rapidly towards unity over the first few hundred nanometers from the GNP surface.

In Fig. 3 all available data have been included, where data that failed to pass the plausibility tests are marked by open symbols. It can be seen that these data are at the extremes of the spread of results, which suggests that corrections of the unidentified normalization issues might further reduce the deviations between the results, both for the narrow beam and for the extended beam with CPE and SPE conditions.

In 1, the uncertainties for the DERs for the confined photon beam were estimated from a two-sided 95% coverage interval for the spread of results obtained by different participants (assuming a log-normal distribution) that was interpreted as the 95% confidence interval. The upper limit of this confidence interval was typically larger than the lower limit by about a factor of two. As in Fig. 3 the spread of results for the extended beam is much smaller than for the narrow beam geometry, a

normal rather than a log-normal distribution may be assumed when estimating the uncertainty of the DER of an extended photon beam from the scatter of results.

However, in this case the corrections for CPE and SPE and the approximations that they imply constitute another source of uncertainty to be accounted for. Fig. 1 shows that the applied CPE and SPE corrections change the dose-per-fluence ratios by more than three orders of magnitude. Hence, the uncertainties associated with the corrections may be expected to be substantial and are discussed in the next Section.

3.2. Uncertainty of the CPE and SPE corrections

The first assumption, which is the basis of the correction for lack of CPE, neglects the so-called sink effect of the GNP 21, i.e. that electrons traversing the GNP will lose more energy than when traversing the same volume of water. This will lead to a reduction of the energy deposited in the water around the GNP. However, taking into account the underestimation of one or more orders of magnitude of absorbed dose to water without the GNP, as seen in Fig. 1(a), the uncertainty introduced by neglecting this effect is probably insignificant. The second implicit assumption involved in the correction for lack of CPE is that the photon mass attenuation and mass absorption coefficients taken from the NIST data bases 12, 18 are the same values as would be obtained from the interaction cross section data implemented in the MC codes. The associated uncertainty can be assumed to be mostly determined by the uncertainties of

Table 2 Ratios of the collision kerma due to interactions of the first generation of scattered photons calculated for isotropic scattering and for the angular distributions from the Klein-Nishina and Thomson cross sections for incoherent and coherent photon scattering. The values were calculated from Table 3 in 16. (The 50 kVp and 100 kVp spectra in 16 were the same as those used in 1.)

spectrum	water	gold
50 kVp	0.44	0.45
60 kVp	0.51	0.52
100 kVp	0.91	0.81

Table 3 Estimated relative contribution of higher order scattered photons to the total collision kerma, calculated from Table 3 in 16.

spectrum	water	gold
50 kVp	0.41	0.42
60 kVp	0.48	0.49
100 kVp	0.64	0.65

Table 4 Estimated relative uncertainty ($k = 2$) of the total collision kerma related to the sum spectrum of primary and all generations of scattered photons. These estimates are obtained by multiplying the deviation of the entries in Table 2 from unity with the respective entries in Table 3.

spectrum	water	gold
50 kVp	0.23	0.23
60 kVp	0.24	0.23
100 kVp	0.06	0.13

the interaction cross sections implemented in the codes which are in the order of a few percent 22.

The correction for lack of SPE, on the other hand, contains two potential sources for large uncertainties. One is related to the approximation of the fluence spectrum of all generations of scattered photons, assuming that the ratio of the total fluence to the fluence of the first generation is the same as that for the hypothetical case that photon scattering was isotropic. The second source of uncertainty is using only the information of the collision kerma rather than the full photon spectrum.

The uncertainty from the approximation used to estimate the fluence of higher-order scattered photons can be estimated by considering the change in the predicted collision kerma from first generation scattered photons when isotropic scattering is assumed. The results are shown in Table 2 as the ratio of the calculated collision kerma for isotropic scattering to that obtained by assuming angular distributions according to the Thomson formula and the Klein-Nishina formula for coherent (Rayleigh) and incoherent (Compton) scattering 16.

For the 50 kVp spectrum, this ratio is 44% for water and 45% for gold. This suggests that if the same factor would also apply to all generations of scattered photons, the fluence contribution from higher order scattered photons could be up to a factor of about 2.2 higher. Or, in other words, that the estimated contribution from higher generations of scattered photons may have an uncertainty as high as 55%, if one assumes the deviation

of aforementioned ratio from unity to define the 95% confidence interval. Together with the fraction of the collision kerma coming from higher order scattered photons (listed in Table 3), the resulting overall relative uncertainty for the estimated collision kerma is in the order of 23% for the 50 kVp spectrum (Table 4). For the 100 kVp spectrum this overall uncertainty contribution is almost a factor of 2 lower. The values for the 60 kVp X-ray spectrum that are also shown in Table 2, Table 3 and Table 4 were derived from simulations performed for this spectrum by participant G1 in the same way as those reported in 1 for the other two radiation qualities.

To estimate the second uncertainty contribution, that comes from using only the condensed information of the collision kerma instead of the detailed spectrum, we consider the superposition of two photon fluence spectra where the resulting dose contribution from photon interactions with the GNP is known. For this purpose, we assume the hypothetical case that the fluence spectrum of all generations of scattered

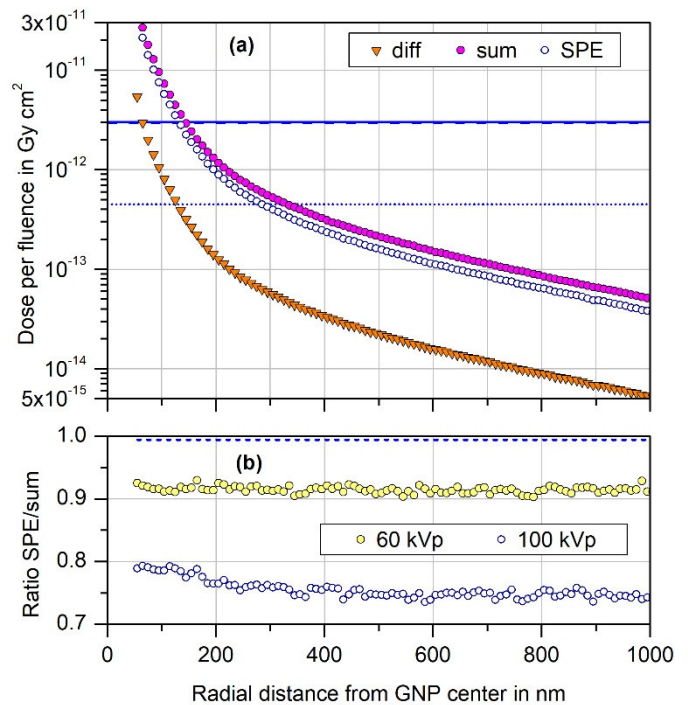


Fig. 4: (a) Difference of the simulation results for a 100 nm GNP present or absent in water traversed by a circular 100 kVp photon beam of diameter 110 nm (downward triangles). The open circles are the corrected values obtained by estimating the contribution of scattered photons with the procedure described in Section 2.3. The filled circles are obtained if the scattered photon spectrum is given by the primary 50 kVp spectrum multiplied by a factor such as to give the same collision kerma in gold as for the open circles. The horizontal lines indicate the dose per fluence to water if CPE (dotted) and SPE (solid, dashed) exist. (b) Radial variation of the ratio of the excess dose per fluence due to photon interactions with the GNP calculated with the estimated scattered photon spectrum to the one obtained with the scaled 50 kVp spectrum. Open circles indicate the ratio of the data shown in the upper part of the figure as open and filled circles. Filled circles indicate the corresponding ratio that is obtained for the 60 kVp primary spectrum when using a scaled 50 kVp spectrum instead of the scattered photon spectrum obtained with the procedure in Section 2.3. The dashed lines indicates the ratio of the values of dose per fluence to water obtained with the scattered photon spectrum according to Section 2.3 to that obtained with the scaled 50 kVp spectrum, both for the case of the 100 kVp primary spectrum.

photons for both the 60 kVp and 100 kVp primary photon spectra is given by the 50 kVp X-ray spectrum multiplied by a factor. This scaling factor is chosen such that the extra collision kerma per fluence of primary photons has the same value as was obtained with the estimated spectrum from section 2.3.

The results obtained are shown in Fig. 4(a). The collision kerma in the GNP is symbolized by the downward triangles for the case of the primary 100 kVp photon spectrum. The corrected values according to section 2.3 and the assumed scaled 50 kVp photon spectrum are indicated by the open and full symbols, respectively. The ratio of the two quantities (shown as open symbols in Fig. 4(b)) is only slightly varying with distance from the GNP and deviates from unity by up to 25%. Using the same approach for the 60 kVp spectrum, and substituting a scaled 50 kVp spectrum for the scattered photon spectrum as obtained from Section 2.3, leads to a ratio of the collision kermas shown by the filled symbols in Fig. 4(b), which deviates from unity by only about 10%. For the collision kerma in water, the ratio of the values obtained with the estimated scattered photon spectrum is close to unity (dashed line in Fig. 4(b)).

The deviations from unity of the data shown in Fig. 4(b) can be taken as estimate for the uncertainty due to a potential variation of the fluence spectrum of higher-order scattered photons with respect to the first generation of scattered photons. Using this approach, the overall combined uncertainty due to the correction for SPE is estimated to be about 25% for both of the considered X-ray spectra. For the 50 kVp primary photon

spectrum, the dominant uncertainty contribution is given in Table 4, whereas for the 100 kVp spectrum the potential change in the photon spectrum dominates.

3.3. Uncertainty of the DERs for an extended field.

Fig. 5 shows the results for the extended beam presented as deviation from unity of the DER for irradiation under secondary particle equilibrium. The symbols are the same data as in Fig. 3, while the dot-dashed line shows the mean of the DERs coming from data that passed the plausibility tests, which were marked by full symbols in Fig. 3. This mean constitutes the best estimate of the DER under secondary particle equilibrium for the four combinations of GNP size and photon spectrum.

All extended-beam data marked by full symbols in Fig. 3 agree within significantly less than 25% with their mean value so that the additional uncertainty coming from the scatter of results from different participants does not significantly increase the uncertainty of the DER (as long as those results that fail the plausibility tests are excluded). The grey shaded area represents the uncertainty band for 95% coverage with this slightly increased uncertainty.

The presentation of the deviation from unity of the DER is better suited for appreciating the range where significant dose enhancement occurs. It is perhaps a more appropriate way of presenting the results, as a GNP leads to additional energy deposition in its vicinity and the DER is by definition unity in absence of a GNP. Furthermore, it elucidates the fact that the

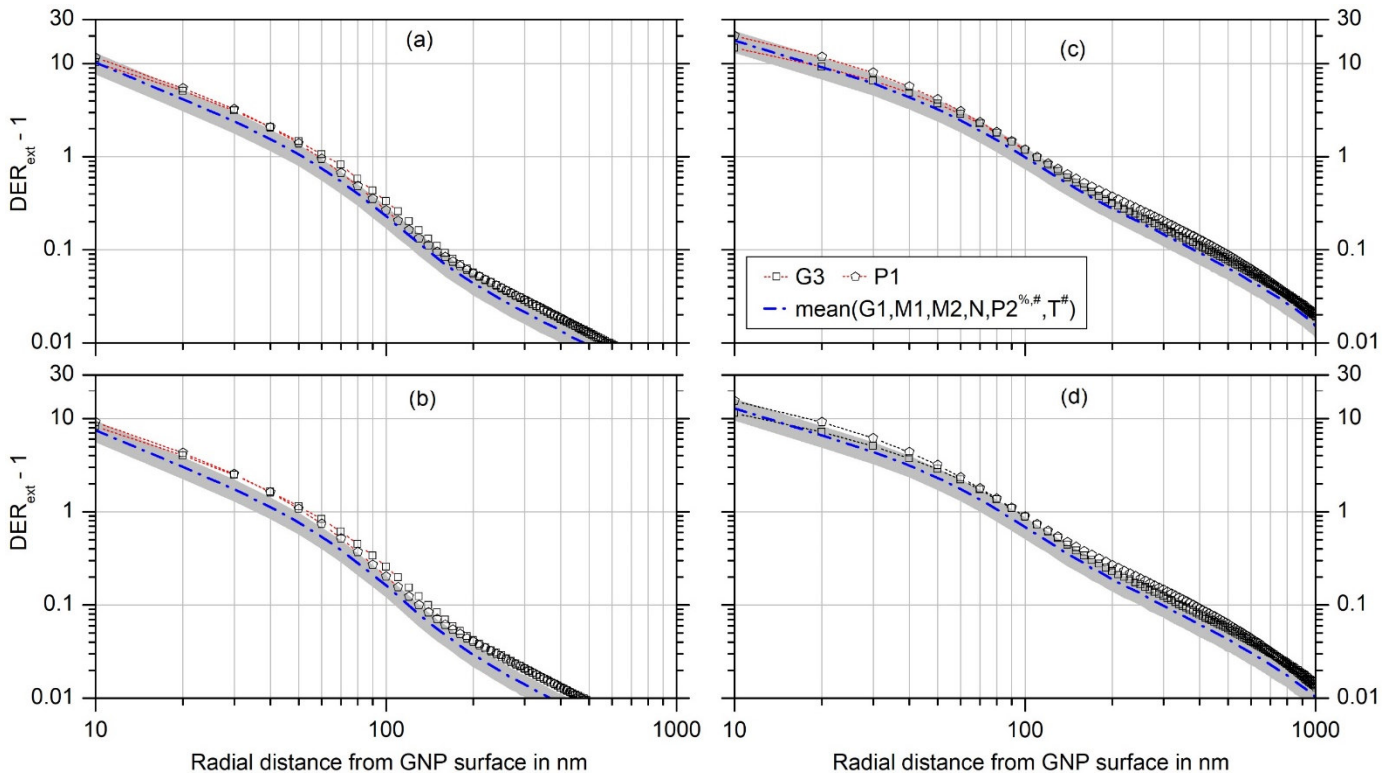


Fig. 5: Deviation from unity of the dose enhancement ratio (DER) for an extended photon field under secondary particle equilibrium for (a) a 50 nm GNP and 50 kVp X-rays, (b) a 50 nm GNP and 100 kVp X-rays, (c) a 100 nm GNP and 50 kVp X-rays and (d) a 100 nm GNP and 100 kVp X-rays. The different symbols correspond to the different participants in the exercise. Open symbols indicate that the reported simulation results did not pass the plausibility checks and no explanation could be reported by the participant. The other data sets passed the plausibility tests, where in some cases identified normalization issues have been corrected for (indicated by a hashtag). The dot-dashed line is the arithmetic mean of all data derived from simulation results that passed the plausibility tests, and the grey shaded area indicates the estimated 95% uncertainty band considering the scatter of these data and the uncertainties of the procedure used for correcting the lack of secondary photon equilibrium in the simulations.

datasets that do not pass the plausibility checks seem to have almost constant offsets from the dot-dashed line in the log-log presentation, i.e. the deviations from unity of the DERs have an almost constant ratio over the radial range shown. This supports the idea that the spread of all results would be significantly smaller if the normalization problems could be identified and corrected.

4. Conclusion

In our paper 1 an intermediate state of the analysis of the code intercomparison exercise was shown with a focus on elucidating potential differences between codes and their application. For this reason, DER results were shown that were directly calculated from the simulation results. In this Comment we have used an approximate correction procedure to derive the DERs that would be found for an extended photon field where secondary particle equilibrium is ensured. These DERs are significantly deviating from unity only within the first few hundred nanometers from the GNP surface and have maximum values in the order of magnitude 10 (Fig. 3).

In addition, an estimate of the uncertainty related to the corrections applied has been presented that amounts to about 25% of the deviation of the DER from unity (at 95% confidence level). If datasets where plausibility checks indicated remaining normalization issues are excluded, the scatter of results between different participants does not significantly increase this uncertainty. However, this uncertainty is about an order of magnitude higher than what is generally considered acceptable for dosimetry in radiotherapy. Therefore, simulations ensuring secondary particle equilibrium are needed to fully assess the uncertainty based on deviations of results between codes only. Such simulations are currently in progress as part of the preparation of a follow-up exercise on multiple GNPs distributed around a cell nucleus 1.

Acknowledgements

This work was, in part, funded by DFG under grant number 386872118. Werner Friedland and Chun Yan Li are acknowledged for providing their simulation results without claiming co-authorship.

References

- [1] Li W B, Belchior A, Beuve M, Chen Y Z, Maria S D, Friedland W et al.. Intercomparison of dose enhancement ratio and secondary electron spectra for gold nanoparticles irradiated by X-rays calculated using multiple Monte Carlo simulation codes. *Physica Medica* 2020;69:147-163.
- [2] Rühm W, Bottollier-Depois J F, Gilvin P, Harrison R, Knežević Ž, Lopez M A et al.. The work programme of EURADOS on internal and external dosimetry. *Annals of the ICRP* 2018;47:20-34.
- [3] Rühm W, Ainsbury E, Breustedt B, Caresana M, Gilvin P, Knežević Ž et al.. The European radiation dosimetry group – Review of recent scientific achievements. *Radiation Physics and Chemistry* 2020;168:108514.
- [4] Hainfeld J F, Slatkin D N, Smilowitz H M. The use of gold nanoparticles to enhance radiotherapy in mice. *Physics in Medicine and Biology* 2004;49:N309-N315.
- [5] Mesbahi A. A review on gold nanoparticles radiosensitization effect in radiation therapy of cancer. *Reports of Practical Oncology & Radiotherapy* 2010;15:176-180.
- [6] Jain S, Hirst D G, O'Sullivan J M. Gold nanoparticles as novel agents for cancer therapy. *The British Journal of Radiology* 2012;85:101-113.
- [7] Dorsey J F, Sun L, Joh D Y, Witztum A, Zaki A A, Kao G D et al.. Gold nanoparticles in radiation research: Potential applications for imaging and radiosensitization. *Translational Cancer Research* 2013;2:280-291.
- [8] Schuemann J, Berbeco R, Chithrani D B, Cho S H, Kumar R, McMahon S J et al.. Roadmap to Clinical Use of Gold Nanoparticles for Radiation Sensitization. *International Journal of Radiation Oncology • Biology • Physics* 2016;94:189-205.
- [9] Her S, Jaffray D A, Allen C. Gold nanoparticles for applications in cancer radiotherapy: Mechanisms and recent advancements. *Advanced Drug Delivery Reviews* 2017;109:84-101.
- [10] Cui L, Her S, Borst G R, Bristow R G, Jaffray D A, Allen C. Radiosensitization by gold nanoparticles: Will they ever make it to the clinic?. *Radiotherapy and Oncology* 2017;124:344-356.
- [11] Kuncic Z, Lacombe S. Nanoparticle radio-enhancement: principles, progress and application to cancer treatment. *Physics in Medicine and Biology* 2018;63:02TR01.
- [12] Hubbell J H., Seltzer S M. Tables of X-Ray Mass Attenuation Coefficients and Mass Energy-Absorption Coefficients from 1 keV to 20 MeV for Elements Z = 1 to 92 and 48 Additional Substances of Dosimetric Interest (version 1.4). National Institute of Standards and Technology, Gaithersburg, MD, 2004; <https://dx.doi.org/10.18434/T4D01F> (Accessed date: 16 March 2020).
- [13] Zygmanski P, Liu B, Tsiamas P, Cifter F, Petersheim M, Hesser J et al.. Dependence of Monte Carlo microdosimetric computations on the simulation geometry of gold nanoparticles. *Physics in Medicine and Biology* 2013;58:7961-7977.
- [14] Zygmanski P, Sajo E. Nanoscale radiation transport and clinical beam modeling for gold nanoparticle dose enhanced radiotherapy (GNPT) using X-rays. *The British Journal of Radiology* 2016;89:20150200.
- [15] Gadoue S M, Zygmanski P, Sajo E. The dichotomous nature of dose enhancement by gold nanoparticle aggregates in radiotherapy. *Nanomedicine* 2018;13:809-823.
- [16] Rabus H, Gargioni E, Li W B, Nettelbeck H, Villagrana C. Determining dose enhancement factors of high-Z nanoparticles from simulations where lateral secondary particle disequilibrium exists. *Physics in Medicine and Biology* 2019:.
- [17] ICRU. Fundamental quantities and units for ionizing radiation (ICRU Report 85). International Commission on Radiation Units and Measurements, Bethesda, MD, 2011.
- [18] Berger M. J., Hubbell J. H., Seltzer S. M., Chang J., Coursey J. S., Sukumar D. S. et al. XCOM: Photon Cross Section Database version 1.5). National Institute of Standards and Technology, Gaithersburg, MD, 2010; <https://dx.doi.org/10.18434/T48G6X> (Accessed date: 16 March 2020).
- [19] Li Wei Bo, al. et. Intercomparison exercise on Monte Carlo simulations of the dose enhancement by a single gold nanoparticle under X-ray irradiation *EURADOS Report, in preparation*.
- [20] Li W B, Beuve M, Maria S D, Friedland W, Heide B, Klapproth A P et al.. Corrigendum on Li et al., Intercomparison of dose enhancement ratio and secondary electron spectra for gold nanoparticles irradiated by X-rays calculated using multiple Monte Carlo simulation codes. *Physica Medica* 2020;69:147-163.. *Physica Medica* submitted:.
- [21] Brivio D, Nguyen P L, Sajo E, Ngwa W, Zygmanski P. A Monte Carlo study of I-125 prostate brachytherapy with gold nanoparticles: dose enhancement with simultaneous rectal dose sparing via radiation shielding. *Physics in Medicine and Biology* 2017;62:1935-1948.
- [22] Andreo P, Burns D T, Salvat F. On the uncertainties of photon mass energy-absorption coefficients and their ratios for radiation dosimetry. *Physics in Medicine and Biology* 2012;57:2117-2136.